Chapter 6: Discussion

Numerous stainless steel samples discussed in the preceding chapters displayed similar results, and therefore this separate discussion chapter will be used to further analyse and discuss the implications of the results obtained and presented in Chapters 3-5. This necessitates a brief summary of the results obtained, as follows:

The stainless steel 316L tests (Chapter 3) generally show the presence of a lithium spinel containing chromium, the corrosion layer covers the full sample, but often features of the bulk, such as grain boundaries, can be observed in the BSE images, e.g. Figure 3.11. The three week tests in Chapter 3 showed what at first were believed to be anomalous results, with the formation of a thick black porous corrosion layer on the sample which is made up of numerous different metal oxides, including iron and chromium oxide. This was further observed in Chapter 4, when tests were conducted to determine the role of lithium in corrosion of stainless steel 316L in molten salts. When the three week tests were repeated the SEM/EDX data in both Chapters 3 and 4 show that the corrosion layer has reverted back to that which is seen in the one week test, with the presence of a layer containing chromium and oxygen.

Generally when the cross section can be analysed, the surface shows the presence of a thin corrosion layer, which reiterates the surface SEM analysis. Some of the results, i.e. for six week test (Figure 3.15), and four week tests (Figure 4.12), show the formation of a double corrosion layer, with an iron oxide product diffusing into the bulk. Finally, an iron chloride is present intermittently on the surface of the repeated three and six week test samples, (Figure 3.12 and Figure 3.13 respectively). It is possible that it is also present in the four week test, but was not visible in the areas of the sample that were imaged.

Tests in molten salts with and without lithium, at a slightly higher temperature (700 °C), yielded results that are comparable to those obtained in Chapter 3. The ternary LiCl-NaCl-KCl tests, show the presence of a lithium chromium oxide corrosion layer as seen in Chapter 3. It also appears that iron-containing crystals have formed on the surface (Figure 4.6) after 3 and 6 weeks in a ternary salt.

The binary NaCl-KCl tests (other than the three week tests) consistently show a thick corrosion layer and the formation of blocky crystals, which gradually increase in size as immersion time increases. The corrosion layer does not cover the full sample, as seen in the ternary test. The repeated three and four week tests also show the presence of iron oxide. Again an anomalous result is seen in the three week tests, with the formation of a thick black corrosion layer. This was difficult to analyse due to its highly

textured surface, but the BSE image shows the presence of long thin crystals, and spot analysis indicates the presence of sodium, iron and oxygen in the corrosion layer.

Further tests were conducted to see how elemental changes within an alloy can effect corrosion. Stainless steel 304L shows similar results to the stainless steel 316L sample, but the corrosion layer does not form as readily. Table 5.1 shows the chromium, and iron content for each of the samples before testing. The chromium content increases by 2 wt. % comparing 304L to 316L, and LDX2101 has a significantly larger increase in chromium content compared to both stainless steel 304L and 316L, by approximately 3 and 5 wt. % respectively. LDX2101 shows the formation of a thick corrosion layer over the surface, with lithium, chromium and oxygen present. The corrosion layer does not adhere well to the surface, and there is also evidence from the cross section analysis that iron oxide has penetrated the bulk. Finally, iron was tested and showed relatively good results, considering its lack of alloying elements.

Table 6.1: composition of major alloy constituents (in wt. %) in the four samples used in Chapter 5.

	Fe	**Cr**	**Other**
Stainless steel 316L	69.59	16.36	14.05
Stainless steel 304L	71.23	18.31	10.46
LDX2101	71.20	21.42	7.38
Iron	99.69	0.04	0.27

Each of the tests conducted on stainless steel 316L at three weeks show unusual results compared to the other time points for the same steel; the stainless steel 316L tests in Chapter 3 show the formation of five corrosion products, each with different structures and elemental compositions, but when this test was repeated using the exact same conditions the corrosion product reverted back to what was observed after one day and one week, occasionally with the addition of an iron compound, which appeared to penetrate the bulk. The three week lithium tests also show anomalous results, with the ternary tests forming iron crystals, which carried on through to the four week tests. Finally, the sample from the three week binary test is covered in a long thin corrosion product which is predominantly made up of iron, oxygen and sodium.

This chapter will focus on the formation of the corrosion products, the formation of spinels, and the tendency of different elements to be present within the spinel. It will also investigate the three week tests and the role of lithium in the form of protective spinel coatings.

6.1: Formation of Corrosion Products

Throughout this work the major corrosion product that has been formed is lithium chromium oxide $LiCrO_2$, which appears as a smooth layer over the stainless steel product.

In addition to this, numerous other products were also formed; chromium oxide (Cr_2O_3), iron (II, III) oxide (Fe_3O_4), iron (II) oxide (FeO), iron (III) oxide (Fe_2O_3), and chromium iron oxide. This section will assess the likelihood of formation of each of these products in standard conditions.

The standard Gibbs free energy of formation is the change in Gibbs free energy when one mole of a substance is formed from its standard constituent elements in their standard states. [1] The Gibbs free energy of formation indicates if it is thermodynamically favourable to form a compound. If the Gibbs free energy of formation is negative it is more likely to form, but this does not take into account kinetic effects [2].

Table 6.2: Gibbs free energies of formation for corrosion products formed in this work; all are given at 298.15 K and 1 atm.

	Gibbs free energy of formation $\Delta G_f°$ (kJ/mol)
Cr_2FeO_4[3]	-1343.8
Cr_2O_3[3]	-1058.1
Fe_3O_4[3]	-1015.4
$LiCrO_2$[4]	-895.6
Fe_2O_3 [3]	-742.2
$FeCl_2$[3]	-302.3
FeO [5]	-251.4

The results in Table 6.2 are given in the order in which they are likely to form based on these Gibbs energies, with Cr_2FeO_4 being more likely to form compared to FeO. In addition to the low likelihood of $LiCrO_2$ forming via its constituent parts, Table 6.2 also shows that the compounds formed in the anomalous stainless steel results in Chapter 3 have a more negative Gibbs free energy of formation, compared to $LiCrO_2$. Therefore the results that were classed as anomalous do agree with the thermodynamic results, and there must be other mechanisms in place to account for the preferential formation of $LiCrO_2$.

The data presented in Table 6.2 do not fully correlate with the results shown in this work, as this approach does not take into account preferential leaching of elements from the samples or the kinetics of the system.

6.2: Annual Corrosion Rate

The annual rate of corrosion can also be calculated from the results given in Chapter 3-5. Due to the significant error associated with these samples this will be an estimate, but general trends can be discussed.

Table 6.3: the average weight changes (g) for the tested samples in Chapters 3 and 5, along with an estimate of the annual corrosion rate (g/year)

Alloy	One week (g)	Annual corrosion rate (g/year)	Three weeks (g)	Annual corrosion rate (g/year)	Four weeks (g)	Annual corrosion rate (g/year)	Six weeks (g)	Annual corrosion rate (g/year)
Stainless steel 316L	-0.4945	-25.7	-1.2399	-21.5	-1.3956	-18.1	-2.4691	-21.4
Stainless steel 304L	-0.3967	-20.6	-0.6253	10.8				
LDX2101	-0.1085	-5.6	0.0069	0.1				
Iron	-0.9890	-51.4	-1.5460	-26.8				

Table 6.4: the average weight changes (g) for the tested samples in different eutectic salts (reported in Chapter 4), along with an estimate of the annual corrosion rate (g/year)

Salt	One week (g)	Annual corrosion rate (g/year)	Three weeks (g)	Annual corrosion rate (g/year)	Three weeks (repeat)	Annual corrosion rate	Four weeks	Annual corrosion rate
Ternary	-0.6012	31.3	-1.7419	30.2	-2.3778	-41.2	-2.1321	-27.7
Binary	-2.2059	114.7	48.5869	842.1	-4.9594	-86.0	-3.0976	-40.3

Table 6.3 shows the annual corrosion rate from chapter 3 and 5, and it can be seen that for all samples the corrosion rate levels out as time progresses, this has been reported before by Richardson et al. [6]. There is an increase in the annual corrosion rate for stainless steel 316L between 4 and 6 weeks, but due to the significant error in the sample masses, it is possible that this is an anomaly.

When the different alloys are compared, it is clear that LDX2101 shows the lowest annual corrosion rate, and although this does look promising it has been attributed to the loss of material due to spalling. Stainless steel 304L again shows a decrease in the annual corrosion rate, with the rate decreasing by almost half between one and three weeks, compared to stainless steel 316L, which only shows a 16% decrease.

Finally, iron shows a large annual corrosion rate, which rapidly decreases by nearly half, but the more interesting result is when the annual corrosion rate for iron and stainless steel 316L are compared. Analysing the results for the three week tests, the annual corrosion rate is only 20% higher for iron compared to stainless steel 316L.

Table 6.4 gives the annual corrosion rate for the samples reported in Chapter 4, and as expected the binary tests give a significantly higher rate of annual corrosion compared to the ternary tests, but it is clear that the rate of corrosion is reducing as time goes on. This reiterates what has been seen previously, where impurities within the salt are used up as time progresses, resulting in a decrease in the corrosion rate [7].

Finally, the ternary results are comparable with those seen in Table 6.3, with a high annual corrosion rate compared to stainless steel 304L and a gradual decrease in the rate as time goes on, if the repeated three week test is omitted.

It should be noted that the mass change also accounts for weight gained via the formation of corrosion products and loss of bulk material and spalling, which can subsequently affect the resultant annual corrosion rate.

6.3: Formation of Spinels

Most of the results reported in the literature review in Chapter 1 showed that exposing stainless steel to a molten salt resulted in the leaching of chromium out of the steel, forming chromium oxide [8-11], but some of these previous studies do mention the formation of sodium and lithium spinels [12, 13]. One author observed enhanced corrosion in stainless steel due to the formation of Na_2CrO_4 after chromium oxide (Cr_2O_3) reacted with NaCl present within the salt [12], and another observed the formation of a double layer with $LiFeO_2$ forming over Cr_2O_3 after 72 hours [13]. It should be noted that the inner layer is penetrating the bulk during corrosion [14]; this is also observed in Chapter 3, where a lithium chromium oxide is formed over an iron oxide layer (Figure 3.15).

The broader literature does indicate that although the solid-state reaction method is the most conventional method to form spinels, molten salts can also be utilised. Kim et al. give an example of this with the formation of $LiNi_{0.5}Mn_{0.5}O_4$ using LiCl and LiOH salts [15], and further work by numerous authors suggests that this is a viable method for spinel formation [16-18].

Frangini et al. [19] also suggest a molten salt synthesis method to form a protective perovskite based layer on stainless steel 316L to be used in molten carbonate fuel cells (MCFC); molten carbonates are used and stainless steel is the source of chromium and/or iron [19]. Although perovskites are not spinels, the idea that a protective ceramic layer can be formed from the constituents of the stainless

steel was implemented successfully. Frangini et al. [19] used a double layer system, with a perovskite layer (La_2O_3) grown over a $LiFeO_2$ layer. The $LiFeO_2$ was used to prevent any initial corrosion during perovskite growth. It was also found that the perovskite could provide excellent corrosion resistance. It was also suggested by Frangini et al. that using an in-situ molten salt synthesis method could be an effective way of coating a sample as it could lead to an impervious oxide barrier [19]. This has been confirmed in some of the work in this thesis, where a lithium chromium oxide has formed over the sample, appearing to prevent further attack from the molten chloride.

Biedenkopf et al. [20] state that molten salt corrosion of a stainless steel with a high chromium content >20 wt. % in a lithium carbonate-potassium carbonate melt results in the formation of $LiFeO_2$ over $LiCrO_2$ [20]. This is in direct contrast to observations in this thesis (Figure 3.15 and Figure 4.13) where iron appears to be diffusing into the bulk and $LiCrO_2$ is present on top. Due to differences in experimental methods including the salt (a molten lithium-potassium carbonate), the temperature (650°C) and the different compositions of the steel, the work by Biedenkopf et al. is not directly comparable with Chapters 3-4, therefore it is possible that there is a change in the formation of the corrosion product, but why this has happened is yet to be determined.

Cheng et al. [21] found that steel in an alkali-nitrate environment formed two layers, $LiFeO_2$ over $(Fe,Cr)_3O_4$ [21]; this is analogous to results obtained in this work, as it proves that it is possible for a lithium metal oxide to form over a metal oxide. Kruizenga and Gill [22] investigated stainless steel 321 in a molten nitrate salt and found that an iron oxide had formed over a mixed chromium iron oxide. This was dependent on temperature, as above 500°C iron oxide was present in the outer layer whereas above 600°C the double layer is lost and sodium ferrite was the main compound present, and it was also noted that at higher temperatures surface spalling was an issue [22]. From this work it can be deduced that differing experimental methods can lead to the loss of the double layer, therefore the presence of the double corrosion layer seen in the six week test and the lack of the double corrosion layer in the one week test is likely due to the different experimental methods used in each test, more than likely the extended time frame. [22].

Numerous sources have stated that the formation of a stable corrosion layer is difficult to obtain in a molten chloride environment, as chlorides act as a fluxing agent [10, 23, 24]. The formation of spinels allows a protective layer to form over the surface of the sample; some work reports that the protective metal oxides which are usually formed in chloride-free systems, but which cannot be stable in the presence of chlorine, are present as the inner layer of a double layer structure [13]. Stainless steels form a passive oxide film on the surface but in the presence of fluoride or chloride ions the film is unstable due to the redox reactions [25]. It is therefore unusual that the samples exposed to ternary

molten salts have formed a protective spinel coating. The formation of a protective spinel is seen in this work along with the formation of a double layer, although differences are present when compared to the literature, namely the presence of a lithium chromium oxide in the upper layer and an iron oxide beneath. Numerous differences in the experimental work in Chapters 3, 4 and 5 compared to the work of Biedenkopf et al., Frangini et al. and Cho et al. [13, 19, 23] could explain the differences in the characteristics of the corrosion layer formed, and investigating this further should give some insight into the formation of the double corrosion layer.

6.4: Role of Lithium

From numerous literature sources it appears that the presence of lithium aids in the formation of a stable corrosion product [19, 20, 26], and this is further suggested in the work presented in Chapter 4, which shows the formation of a uniform corrosion layer over the surface of the ternary samples compared to the samples tested in a binary salt, where an unstable corrosion layer is formed. Further work by Biedenkopf et al. [23] showed that when testing eight low and high alloy steels in a lithium carbonate-potassium carbonate melt, lithium iron oxide ($LiFeO_2$) is formed on top of mixed oxides containing iron and chromium. It was suggested by those authors that the lithium iron oxide protects the steel from further attack, and it was shown that the outer lithium-containing layer grows via outward diffusion, whereas the inner layer is formed via inward growth [23]. Due to the inner corrosion layer in this work penetrating the bulk, it is likely that this growth mechanism has taken place.

Merwin and Chidambaram [27] investigated the effect of lithium on the corrosion of stainless steel 316L exposed to molten LiCl-Li_2O-Li. It was found that a variation in the Li concentration affected the corrosion product: at low concentration (0.2-0.4 wt. %) a lithium chromium oxide layer formed over the surface. The corrosion of stainless steel 316L is dependent on the formation of this layer, whereas a Li concentration of 0.6 wt.% resulted in the formation of an unstable layer with chromium leaching [27]. Although the Li^0 concentration was not monitored in this work, the work of Merwin and Chidambaram does show that a small variation in the lithium concentration could result in the formation of different corrosion products.

6.5: Apparent Anomalous Results Obtained in Three Week Tests

Unusual results were obtained in the initial three week tests (Sections 3.2.2.3 and 3.2.2.4) and the three week binary test (Figure 4.9); the initial three week test in Chapter 3 test generated five different corrosion products, whereas the three week binary test incorporated sodium instead of lithium in the corrosion product. Initially, these results appear anomalous, but it is suggested in other work [10, 12, 28] that a stable corrosion layer cannot be formed on the surface of an alloy in the presence of molten

alkali halides when impurities, such as oxygen, are present. Therefore it is possible that the results that at first appear to be anomalous are actually what could have been the expected results, as the protective layer is unable to withstand the molten salts corrosive attack. Numerous sources have stated that within a closed molten alkali fluoride system there is a change in the corrosion rate after 500 hours (i.e. 3 weeks), at which time the impurity level reached a steady state, assuming a closed system, resulting in a decrease in the corrosion rate [6, 29, 30]. It was therefore anticipated before experimental work began that three week tests would show interesting results. This is the case in Chapters 3 and 4 as these samples show completely different corrosion products at three weeks compared to the previous results (1 day and 1 week), and subsequently revert back to the original results during the four week test.

The visual appearance of the corrosion products obtained in the three week initial test and the three week binary test appear to be very similar to results obtained by Sellers et al. [31] when a stainless steel 316L crucible failed during a test of FLiNaK at 850°C causing the salt to react with the silicon carbide insulation. That test was a closed experiment and therefore oxygen ingress was not expected, but small amounts were present in the furnace lining. Sellers et al. stated that it is likely that further oxygen was introduced after the furnace door was opened and resulted in the formation of hematite (α-Fe_2O_3) along with Na_2SiF_4, K_2SiF_6, SiF_6 and F_2 [31]. Figure 1.5 shows an image of the resultant corrosion product. Although it is known that there was no equipment or seal failure in any of the experiments in Chapter 3 and 4, it is thought that the work of Sellers et al. may allow some conclusions to be made. From their EDX data, Sellers et al. state that jagged rough edges contained oxygen, silicon, potassium and iron along with hematite (α-Fe_2O_3), and the smoother areas consist of oxygen, potassium and chromium. It is stated that depletion of iron and chromium along grain boundaries is the main mode of attack, and that the reaction between the molten salt and insulation material resulted in a corrosive vapour being formed. Corrosive attack via vapour entering externally is not possible in the three week tests presented in this work, as the samples were fully submerged in the molten salt and therefore not subjected to any vapours. However, the porous nature of the samples in the work of Sellers et al. is proposed to be due to the sublimation of iron (II) fluoride at 690°C; iron (II) fluoride vapour within the corrosion layer caused expansion and eventual release of vapour [31]. It is unlikely that this mechanism will be seen in a chloride salt as iron (II) chloride sublimes at 700°C in a hydrogen chloride atmosphere [32]. Consequently, due to the temperature of the furnace in the stainless steel 316L tests being 600°C, it is unlikely that the sublimation of iron (II) chloride formed the porous corrosion product observed in the three week stainless steel 316L tests. However, it is possible that iron (II) chloride sublimation is responsible for the voids observed in the cross sectional BSE images observed in the binary three week lithium tests (Figure 4.15) as they were run at 700°C.

Frangini et al. [19] showed that after 400 hours of testing (approximately 17 days) of stainless steel 316L in a lithium-rich molten salt, a blocky corrosion product was formed, and their EDX data indicated that the inner layer $LiFeO_2$ was converted to a mixed (Fe,Cr) oxide due to the reaction of $LiFeO_2$ and the stainless steel 316L at 650°C [19]. The results of Frangini et al. appear to follow a similar pattern to the work conducted in the three week initial and binary lithium tests in this thesis, with the conversion of lithium metal oxide to mixed oxides, but the reason for this is still unclear.

Shankar and Mudali [33] investigated stainless steel in a lithium chloride-potassium chloride melt at 500°C in an argon atmosphere for 24 and 100 hours. They do not explicitly state which corrosion products are formed, but they do identify it as chromium rich and porous, and so it is therefore likely that the product formed is similar to the product of the three week tests shown in this work (Figure 4.16). Shankar and Mudali conducted their experiments in a closed environment, allowing no oxygen to aid in the formation of a protective layer, and the results obtained here reiterate the theory that stable corrosion products cannot be formed in a molten salt environment.

Biedenkopf et al. [23] also suggest that between 50-500 hours, the steel is predominantly attacked by air within the system, and after 500 hours they see the formation of $LiFeO_2$; an image of the microstructure is seen in Figure 6.1, which is similar to Figure 3.17 and Figure 4.10. Although the time frames are different, the microstructure is similar, and this observation further confirms that the presence of oxygen within the salt causes the formation of a corrosion product with this microstructure.

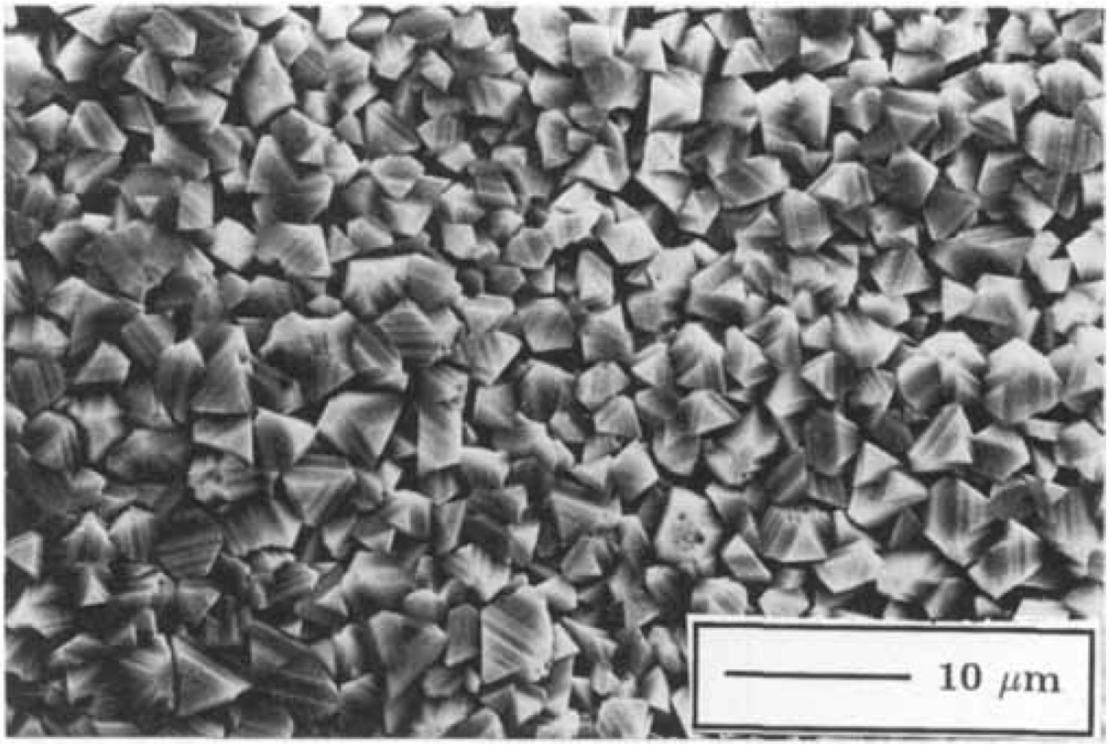

Figure 6.1: $LiFeO_2$ corrosion product formed on the high alloy stainless steel in the work of Biedenkopf et al., reproduced from reference [23].

Further work by Spiegel et al. [14] investigated the different corrosion products formed on high alloy steels in molten carbonate over different time frames; after 50 hours Fe_2O_3 and $FeCr_2O_4$ were formed, between 50-500 hours $LiFeO_2$ and $LiFe_5O_8$, and after 5000 hours $FeCr_2O_4$, $LiFeO_2$ and $FeCr_2O_4$ were observed [14]. This study shows that different corrosion products are formed over different time scales, and although the results are different from what has been observed in Chapter 3-5 of this thesis, where the sporadic formation of a porous corrosion layer is observed at three weeks, it does give an indication that an experimental time frame can result in differing corrosion products.

6.6: Conclusions

As mentioned throughout this work, it is difficult to form a protective layer on an alloy in a molten salt as the corrosion product that forms is not stable this is further confirmed by inspecting the Gibbs free energies of formation of key corrosion products, which suggest that metal oxides are more likely to form. It is therefore postulated that the results obtained in the three week tests are the results that should have been observed throughout this work as the presence of any impurity within the molten salt can cause severe corrosive attack. Sellers et al. and Biedenkopf et al. both showed results similar to those obtained at three weeks, and both state that impurities present within the salt have caused the unstable porous corrosion product to form [23, 31], but the levelling off of the corrosion rate in

this work does suggest that even in an open system, impurities are utilised in the formation of the corrosion product and subsequently not consumed. It appears that lithium aids in the formation of a protective corrosion layer. Occasionally sodium will be utilised, but this does not give the same level of protection as lithium.

Literature cited

1. P. Atkins and J.D. Paula, *Atkins' Physical Chemistry*. 2006: Oxford University Press.
2. T. Matsoukas, *Fundamentals of Chemical Engineering Thermodynamics*. 2012: Pearson Education.
3. D.R. Lide (ed.), *Standard Thermodynamic Properties of Chemical Substances*, in *CRC Handbook of Chemistry and Physics, Internet Version, 2005*. CRC Press, Boca Raton, FL, 2005.
4. S. Dash, Z. Singh, R. Prasad, and D.D. Sood, *Standard molar Gibbs free energies of formation of $LiCrO_2$ and of $NaCrO_2$.* The Journal of Chemical Thermodynamics, 1990. **22**(1): p. 61-66.
5. J.A. Dean, *Enthalpies and Gibbs Energies of Formation, Entropies, and Heat Capacities of the Elements and Inorganic Compounds*, in *Lange's Handbook of Chemistry*. 1999, McGraw Hill. Inc.
6. L.S. Richardson, D.C. Vreeland, and W.D. Manly, *Corrosion of Molten Fluorides.* Oak Ridge National Laboratory, 1952. **ORNL-1491**.
7. J.H. DeVan, *Effect of Alloying Addtions on Corrosion Behavior of Nickel-Molybdenum Alloys in Fused Fluoride Mixtures (thesis)*. 1969, Oak Ridge National Laboratory
8. Y. Shinata, F. Takahashi, and K. Hashiura, *NaCl-induced hot corrosion of stainless steels.* Materials Science and Engineering, 1987. **87**: p. 399-405.
9. L.C. Olson, *Materials Corrosion in Molten LiF-NaF-KF Eutectic Salt*, in *Department of Engineering Physics*. 2009, University of Wisconsin-Madison.
10. K. Sridharan and T.R. Allen, *Corrosion in Molten Salts* in *Molten Salts Chemistry*, H. Groult and F. Lantelme, Editors. 2013, Elsevier: Oxford. p. 241-267.
11. S. Fabre, C. Cabet, L. Cassayre, P. Chamelot, S. Delepech, J. Finne, L. Massot, and D. Noel, *Use of electrochemical techniques to study the corrosion of metals in model fluoride melts.* Journal of Nuclear Materials, 2013. **441**(1–3): p. 583-591.
12. N. Hiramatsu, Y. Uematsu, T. Tanaka, and M. Kinugasa, *Effects of alloying elements on NaCl-induced hot corrosion of stainless steels.* Materials Science and Engineering: A, 1989. **120**: p. 319-328.
13. S.-H. Cho, J.-M. Hur, C.-S. Seo, and S.-W. Park, *High temperature corrosion of superalloys in a molten salt under an oxidizing atmosphere.* Journal of Alloys and Compounds, 2008. **452**(1): p. 11-15.
14. M. Spiegel, P. Biedenkopf, and H.J. Grabke, *Corrosion of iron base alloys and high alloy steels in the Li_2CO_3-K_2CO_3 eutectic mixture.* Corrosion Science, 1997. **39**(7): p. 1193-1210.
15. J.H. Kim, S.T. Myung, and Y.K. Sun, *Molten salt synthesis of $LiNi_{0.5}Mn_{1.5}O_4$ spinel for 5 V class cathode material of Li-ion secondary battery.* Electrochimica Acta, 2004. **49**(2): p. 219-227.
16. R.H. Arendt, *The molten salt synthesis of single magnetic domain $BaFe_{12}O_{19}$ and $SrFe_{12}O_{19}$ crystals.* Journal of Solid State Chemistry, 1973. **8**(4): p. 339-347.
17. D.D. Jayaseelan, S. Zhang, S. Hashimoto, and W.E. Lee, *Template formation of magnesium aluminate ($MgAl_2O_4$) spinel microplatelets in molten salt.* Journal of the European Ceramic Society, 2007. **27**(16): p. 4745-4749.
18. W. Xiao, W. Liu, X. Mao, H. Zhu, and D. Wang, *Chemical mixing in molten-salt for preparation of high-performance spinel lithium manganese oxides: Duplication of morphology from nanostructured MnO_2 precursors to targeting materials.* Electrochimica Acta, 2013. **88**: p. 756-765.

19. S. Frangini, A. Masci, and F. Zaza, *Molten salt synthesis of perovskite conversion coatings: A novel approach for corrosion protection of stainless steels in molten carbonate fuel cells.* Corrosion Science, 2011. **53**(8): p. 2539-2548.
20. P. Biedenkopf, M. Spiegel, and H.J. Grabke, *The corrosion behaviour of iron and chromium in molten $(Li_{0.62}K_{0.38})_2CO_3$.* Electrochimica Acta, 1998. **44**(4): p. 683-692.
21. W.-J. Cheng, D.-J. Chen, and C.-J. Wang, *High-temperature corrosion of Cr–Mo steel in molten $LiNO_3$–$NaNO_3$–KNO_3 eutectic salt for thermal energy storage.* Solar Energy Materials and Solar Cells, 2015. **132**: p. 563-569.
22. A. Kruizenga and D. Gill, *Corrosion of iron stainless steels in molten nitrate salt.* Energy Procedia, 2014. **49**(0): p. 878-887.
23. P. Biedenkopf, M. Spiegel, and H.J. Grabke, *High temperature corrosion of low and high alloy steels under molten carbonate fuel cell conditions.* Materials and Corrosion, 1997. **48**(8): p. 477-488.
24. W.D. Manly, J. G. M. Adamson, J.H. Coobs, J.H. DeVan, D.A. Douglas, E.E. Hoffman, and P. Patriarca, *Aircraft Reactor Experiment- Metallurgical Aspects*. 1957, Oak Ridge National Laboratory.
25. D.F. Williams and L.M. Toth, *Chemical considerations for the selection of the coolant for the advanced high-temperature reactor.* 2005, Oak Ridge National Laboratory: Oak Ridge, Tennessee.
26. P. Biedenkopf, M. Spiegel, and H.J. Grabke, *The corrosion behavior of Fe-Cr alloys containing Co, Mn, and/or Ni and of a Co-base alloy in the presence of molten (Li,K)-carbonate.* Materials and Corrosion, 1997. **48**(11): p. 731-743.
27. A. Merwin and D. Chidambaram, *The effect of Li0 on the corrosion of stainless steel alloy 316L exposed to molten LiCl-Li_2O-Li.* Corrosion Science. **126**: p. 1-9.
28. L.C. Olson, J.W. Ambrosek, K. Sridharan, M.H. Anderson, and T.R. Allen, *Materials corrosion in molten LiF–NaF–KF salt.* Journal of Fluorine Chemistry, 2009. **130**(1): p. 67-73.
29. J.H. DeVan, J.R. DiStefano, W.P. Eatherly, J.R. Reiser, and R.L. Klueh, *Materials considerations for molten salt accelerator-based plutonium conversion systems.* AIP Conference Proceedings, 1995. **346**(1): p. 476-487.
30. A. Nishikata, H. Numata, and T. Tsuru, *Electrochemistry of molten salt corrosion.* Materials Science and Engineering: A, 1991. **146**(1): p. 15-31.
31. R.S. Sellers, M.H. Anderson, K. Sridharan, and T.R. Allen, *Failure analysis of 316L stainless steel crucible by molten fluoride salt interaction with clay bonded silicon carbide.* Engineering Failure Analysis, 2014. **42**: p. 38-44.
32. D.L. Perry, *Handbook of Inorganic Compounds*. 2011: CRC Press. Taylor and Francis Group
33. A.R. Shankar and U.K. Mudali, *Corrosion of type 316L stainless steel in molten LiCl–KCl salt.* Materials and Corrosion, 2008. **59**(11): p. 878-882.